Myosin-independent cytokinesis in *Giardia* utilizes flagella to coordinate force generation and direct membrane trafficking

William R. Hardin[a], Renyu Li[a], Jason Xu[b], Andrew M. Shelton[a], Germain C. M. Alas[a], Vladimir N. Minin[a,b], and Alexander R. Paredez[a,1]

[a]Department of Biology, University of Washington, Seattle, WA 98195; and [b]Department of Statistics, University of Washington, Seattle, WA 98195

Edited by Edward D. Korn, National Heart, Lung, and Blood Institute, Bethesda, MD, and approved June 13, 2017 (received for review March 28, 2017)

Devoid of all known canonical actin-binding proteins, the prevalent parasite *Giardia lamblia* uses an alternative mechanism for cytokinesis. Unique aspects of this mechanism can potentially be leveraged for therapeutic development. Here, live-cell imaging methods were developed for *Giardia* to establish division kinetics and the core division machinery. Surprisingly, *Giardia* cytokinesis occurred with a median time that is ∼60 times faster than mammalian cells. In contrast to cells that use a contractile ring, actin was not concentrated in the furrow and was not directly required for furrow progression. Live-cell imaging and morpholino depletion of axonemal Paralyzed Flagella 16 indicated that flagella-based forces initiated daughter cell separation and provided a source for membrane tension. Inhibition of membrane partitioning blocked furrow progression, indicating a requirement for membrane trafficking to support furrow advancement. Rab11 was found to load onto the intracytoplasmic axonemes late in mitosis and to accumulate near the ends of nascent axonemes. These developing axonemes were positioned to coordinate trafficking into the furrow and mark the center of the cell in lieu of a midbody/phragmoplast. We show that flagella motility, Rab11, and actin coordination are necessary for proper abscission. Organisms representing three of the five eukaryotic supergroups lack myosin II of the actomyosin contractile ring. These results support an emerging view that flagella play a central role in cell division among protists that lack myosin II and additionally implicate the broad use of membrane tension as a mechanism to drive abscission.

actin | Rab11 | PF16 | tubulin | mitosis

Cell division is a fundamental process whereby cellular content is partitioned for proliferation. Drugs that target this process are immensely valuable as cancer therapeutics (1) and have promise for treating infectious disease (2–4). *Giardia lamblia* (synonymous with *Giardia intestinalis* and *Giardia duodenalis*) is a common waterborne pathogen that infects 280 million people each year (5). In addition to being a major parasite, *Giardia* belongs to possibly the earliest diverging eukaryotic lineage and could provide clues about early mechanisms of cell division (6, 7). Despite the fundamental requirement for division to proliferate, the mechanisms underlying cytokinesis vary across the evolutionary tree (8). As *Giardia* has actin but lacks myosin and all known actin cytoskeletal components required for amoeboid motility and cytokinesis (9), it is not clear how the division plane is specified, if division involves force generation for daughter cell separation, or if division occurs strictly through a membrane remodeling mechanism (8).

Our most complete mechanistic understanding of cytokinesis comes from studies of model organisms that are Unikonts, a group that comprises the supergroups Opisthokonta (e.g., yeast to man) and Amoebozoa (e.g., *Dictyostelium discoideum*) (10). Animals use an actomyosin contractile ring to pinch the plasma membrane down onto the midbody microtubules (11). Abscission at the midbody is subsequently completed by plus-end–directed vesicle trafficking to the center of the midbody and ESCRT-III–mediated scission (12). Plants lack myosin II and the pinching down mechanism for scission; instead, extensive membrane trafficking is used to build a new cell wall, known as the cell plate, between daughter cells. After mitosis, interdigitated spindle microtubules maintain antiparallel organization and transition to a cytokinetic apparatus known as the phragmoplast. Microtubules of the phragmoplast guide Golgi-derived vesicles to the center of the division plane by using plus-end–directed trafficking (13). Intriguingly, proteomic analysis has revealed that the phragmoplast shares many molecular components with the mammalian midbody, suggesting that, despite appearances, plant cytokinesis employs a modified midbody mechanism (14).

Discovery of the diverse strategies that cells use to accomplish cell division will provide information on the constraints of eukaryotic cell division. Although the myosin II-based actomyosin contractile ring has a central role in Unikont cytokinesis, cells can divide without myosin II under specific conditions (15–17). *Dictyostelium* and mammalian cells with impaired myosin II function can complete cytokinesis by using traction to pull daughter cells apart (15–17). Hence, the use of myosin II may be implemented on top of a more ancient mechanism that is dependent on cortical tension and a Laplace-like pressure property of cells that serves to minimize the surface area-to-volume ratio (18, 19). Moreover, phylogenetic distribution of myosin II is limited to Unikonts with one known exception that may be an example of horizontal gene transfer (20, 21); thus, three of the five eukaryotic supergroups use an alternative to the canonical "purse-string" mechanism of cytokinesis, as is the case in plants (22). The number and types of alternative mechanisms remain understudied (23), especially in cells that have been difficult to culture and for which molecular and imaging methodologies are lacking.

The study of giardial mitosis and cytokinesis has been challenging because of a lack of effective cell synchronization and live-cell imaging, which is complicated by *Giardia's* lethal sensitivity to

Significance

Many protists, including *Giardia*, lack myosin II and thus are unlikely to use the canonical contractile mechanism of cell division. *Giardia* depends solely on its flagella for motility; here, we show that flagella function is also required to drive daughter cells in opposite directions for cytokinesis. Additionally, just before cytokinesis, Rab11 accumulated in the forming furrow and the nascent intracytoplasmic axonemes were oriented to deliver Rab11. This mechanism constitutes a means to mark the center of the cell and guide trafficking to the furrow. These results support an emerging view that flagella play a central role in cell division among protists that lack myosin II.

Author contributions: W.R.H. and A.R.P. designed research; W.R.H., R.L., A.M.S., and G.C.M.A. performed research; W.R.H. contributed new reagents/analytic tools; W.R.H., R.L., J.X., A.M.S., V.N.M., and A.R.P. analyzed data; and W.R.H. and A.R.P. wrote the paper.

The authors declare no conflict of interest.

This article is a PNAS Direct Submission.

[1]To whom correspondence should be addressed. Email: aparedez@uw.edu.

This article contains supporting information online at www.pnas.org/lookup/suppl/doi:10.1073/pnas.1705096114/-/DCSupplemental.

www.pnas.org/cgi/doi/10.1073/pnas.1705096114

oxygen concentrations greater than 5% (24). Initial studies completely missed the presence of a mitotic spindle, leading to the proposal of several incompatible mechanisms for cell division (25–29). Ultimately, *Giardia's* mitotic stages were found to begin similarly to those of plants and animals (30). The spindle, however, is completely disassembled before cytokinesis, and division occurs across the long rather than the short axis of the cell (30–32). The mechanism for coordinating membrane remodeling during cytokinesis and the timing of major events remain unexplored. Here we combine the use of a hypoxic stage-top incubator, a newly developed low-fluorescence media formulation, and a bright fast-folding fluorescent protein tag (33) that allow robust imaging of *Giardia* throughout the cell cycle. We use these technical advances to uncover the core division machinery and establish a working model for *Giardia's* mechanism of myosin-independent cytokinesis.

Results

Giardia Uses a Tubulin Reservoir to Support Rapid Mitosis and Ventral Disk Assembly. The ability to follow fluorescent proteins in live cells has been one of the most powerful tools for uncovering the mechanism of cytokinesis in model systems (34). To study the dynamics of individual proteins during the cell cycle, we developed a low-fluorescence culture medium that supports cell growth. Our newly formulated medium, SB5050, has a 92% reduction in background fluorescence yet still maintains 35% as many mitotic events as standard media (Fig. S1 and Dataset S1). To follow tubulin dynamics, we tagged the N terminus of β-tubulin with an 18-aa flexible linker and the fast-folding bright fluorescent protein mNeonGreen (33), generating mNeonGreen–C18–β-tubulin (mNG-Tub). *Giardia* has a highly organized microtubule cytoskeleton (Fig. 1*A*), including eight flagella, a ventral adhesive disk (formed from an overlapping sheet of parallel microtubules that facilitates attachment to the host), and a median body (a bundled microtubule structure thought to be a reservoir of tubulin and disk components) (35). Expression of mNG-Tub under its endogenous promoter permitted visualization of microtubules in the ventral disk, median body, flagella, and mitotic spindles (Fig. 1 and Movie S1).

On initiation of mitosis, the flagella and basal bodies rearranged and two independent mitotic spindles nucleated in proximity to the basal bodies (T14; Fig. 1*B*). As the spindles grew in size, the tubulin signal from the median body shrank proportionally (T13–T19). During telophase, the cage-shaped spindles collapsed into tight bundles of microtubules (compare dorsal row T19 and T23 in Fig. 1*B*). Daughter disk assembly was initiated at one end of each spindle in opposing orientations (T23). As the ventral discs continued to grow in size, the spindle was disassembled and nascent flagella grew in the region previously occupied by the spindle (T26). The observed flux of tubulin from the median body to assembling microtubule structures represents experimental support for the previously proposed idea that the median body is used as a reservoir of tubulin (36, 37); however, our results indicate that, in addition to being a reservoir for building the ventral discs (process requiring ∼3 min), the median body supports assembly of the spindle and nascent flagella. Meanwhile, during daughter ventral disk neogenesis, the parental disk disassembled from the interior causing the central microtubule bare area to grow as the disk thinned (T23–T26). When the overlap zone of the disk has disassembled, the disk microtubules straightened, leading to the adoption of an open C-shaped conformation (T27). Furrow ingression coincided with transition to this open conformation. The timing of these events suggests that the parental disk physically impedes furrow progression and its disassembly is tightly coordinated with cytokinesis.

Giardia lacks the machinery for amoeboid motility and depends solely on flagella for locomotion (9, 38). Notably, high-speed imaging has revealed that *Giardia*'s four flagella pairs have different modes of movement. The caudal flagella, which originate near the nuclei and have approximately two thirds of their length running through the cell, are used to undulate the anterior of the cell so that this region acts like a flipper while the anterior and posterolateral flagella generate canonical power strokes (39). Corresponding with the parental disk opening, daughter cells moved in opposition to each other. We propose that caudal flagella flexion (i.e., sustained bending) is important for initiating daughter cell separation. As the intracytoplasmic axonemes of the caudal flagella are nucleated by basal bodies that are intimately associated with the nascent ventral discs (40), this arrangement could facilitate positioning the daughter ventral discs. Indeed, these intracytoplasmic axonemes were observed to flex in opposite directions during cytokinesis, and, as the daughter cells moved in opposite directions, the plasma membrane appeared to stretch around the two new discs and the furrow advanced between them (Fig. 1*B* and Movies S1 and S2). Abscission occurred after daughter cells transitioned into a tail-to-tail orientation and swam in opposite directions, presumably driven by anterior flagella power strokes. After scission, daughter cells quickly attached to the cover glass, indicating that the nascent ventral discs are functional upon cytokinesis despite the immaturity of the ventral flagella, which have been proposed to support attachment (41). Notably, the ventral and posterolateral flagella were observed to grow at different rates (Fig. 1*B* and Movie S1), suggesting that the mechanism of flagella-length control is more complex in *Giardia* than the constitutive regulatory mechanism of *Chlamydomonas reinhardtii* (42). Also, there was no observed rebuilding of the median body during the time we observed the regrowth of the flagella, supporting the idea that the median body is a microtubule reservoir.

Previous studies of fixed cells found that the start of mitosis is indicated by coordinated chromosome condensation, translocation of the two nuclei to the cell center, and repositioning of basal bodies and their attached flagella to set up the mitotic spindles (30, 32, 43, 44). A prior study that used drugs to partially synchronize cells was able to follow a handful of cells through division by using 40× phase optics and found that mitosis and cytokinesis took ∼50 min (32). By using long-term 4D differential interference contrast (DIC) imaging in the absence of any drugs, we find that mitosis and cytokinesis occurred in ∼7.5 min (Fig. S2*A* and Movie S3), much faster than the original estimate made without temperature or atmospheric control (32). The median time between mitosis to the initiation of cytokinesis was 6 min 28 s (n = 93; Fig. S2*B*). Remarkably, the median time for cytokinesis was 50 s (n = 130; Fig. S2*C*), with 89% of cells completing cytokinesis within 2 min. This time is 30–90 times faster than the rates reported for plants, fungi, and mammalian cells (23, 45–47). Intriguingly, *Dictyostelium* myosin II mutants divide in approximately half the time of their WT counterparts (6–8 min), suggesting that the myosin II-based cytokinesis may have arisen for increased fidelity rather than speed (48). The previously observed doubling time for the strain WBC6, used in this study, was ∼8 h; thus, our timing is precisely in agreement with the mitotic index of 1.3% observed in nonsynchronized cultures (6.5 min/480 min = 0.013) (30, 49). Cleavage furrow ingression measurements were averaged by randomly sampled locally estimated scatterplot smoothing (LOESS) curves; ingression is fastest after initiation and then progresses at a steady rate and is followed by a slower final scission event (Fig. 1*C* and Fig. S2 *D* and *E*). This nonuniform rate may indicate a requirement for the sequential action of multiple cell-division components that cooperate together to achieve furrow ingression and abscission.

Flagella Are Required for Cleavage Furrow Formation and Abscission. Myosin II mutants of *Dictyostelium* were shown to use ameboid motility to crawl apart for cytokinesis (17). Organisms that lack myosin II and depend on their flagella for motility, such as *Trypanosoma brucei* and *Tetrahymena*, also require motility for abscission (50–52). To address whether the flagella have a direct role in cytokinesis, we treated *Giardia* with small molecule inhibitors that have been shown to disrupt flagellar function in other systems [Ciliobrevin A, Ciliobrevin D, drug E, drug F, and drug P (53–55)]. However, these drugs did not visibly perturb *Giardia* flagella beating or length. We therefore tested the role of the flagella by knocking down Paralyzed Flagella 16 (PF16), a highly conserved key component of the axoneme central pair apparatus (56) required for stabilizing the orientation of the central pair microtubules in

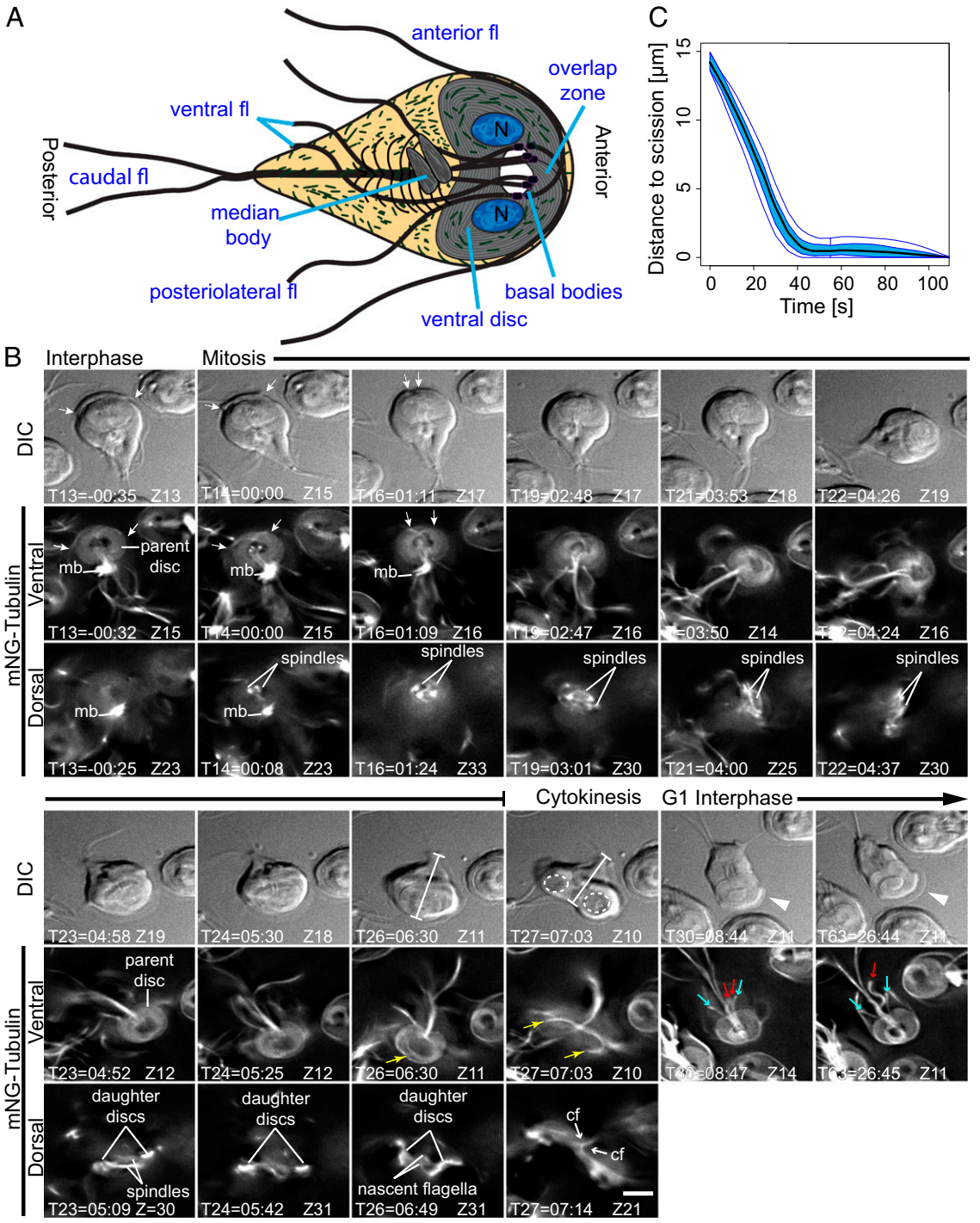

Fig. 1. Characterization of mNG-Tub dynamics over the cell cycle. (*A*) Diagram of cellular features of an interphase trophozoite (n, nucleus; fl, flagella). (*B*) A trophozoite captured from interphase through cytokinesis (T, time in min:s; Z, optical slice). DIC images show orientation and correspond to fluorescent images (ventral and dorsal plane). The onset of mitosis was signified by rearrangement of anterior flagella exit points (white arrows; magnified view in Fig. S2) and nucleation of the spindle (both begin at T14). Concomitant with spindle assembly (dorsal row), the median body (mb) microtubules were depleted (ventral row, T14–T19). The spindles transitioned from basket-shaped to collapsed MT bundles (T21–T23). Construction of daughter ventral discs initiated (T23). The center of the parental disk was depleted of mNG-Tub as daughter discs grew (T26, Z11; yellow arrow indicate overlap zone). Cytokinesis begins at T27 and is completed at T28. (Dashed ellipses, position of the daughter discs; dimension bars mark the trajectory of the furrow; yellow arrows, ends of the now open parental ventral disk.) Note the flexion of the caudal flagella (cf) in opposite directions (T27, Z21). Daughter cells attach to the substrate at T30 (one shown in ventral view). The DIC image shows that the daughter initially lacks a ventrolateral flange, indicating that this structure was consumed during cytokinesis (T30 and more fully formed at T63, white arrowhead). Additionally, posterolateral (blue arrows) and ventral flagella pairs (red arrows) lengthened after division with different growth rates. (Scale bar: 5 µm.) Similar observations were made for at least 10 other mNG-Tub–expressing cells. (*C*) Functional box plot of bootstrapped LOESS curves derived from cleavage furrow measurements (dimension bars in DIC row T26 and T27; also see Fig. S2). Distance to scission is the distance that the furrow has to travel for daughter cell separation; average cells begin with a ~14-µm path length. Data are from 25 randomly selected cells completing cytokinesis within 2 min. Central black line is the mean of the bootstrapped LOESS curves; the blue band indicates the 50% CI bound by 95% confidence bands of bootstrapped distances.

C. reinhardtii (57), mice (58), and *T. brucei* (52). Misorientation of the central pair in *T. brucei* impairs cytokinesis (52). Likewise, a previous study of PF16 in *Giardia*, aimed at testing the role of the flagella in parasite attachment, noted that PF16 knockdown (KD) reduced flagella motility and impaired cytokinesis (41). The nature of this cytokinesis defect, however, was not reported.

To monitor the efficacy of the morpholino KD, we endogenously tagged PF16 with a C-terminal triple-HA epitope tag (59). As expected, PF16-HA localized to the flagella, and quantitative Western blotting revealed 69% depletion at the population level 24 h after morpholino treatment (Fig. 2*A* and Fig. S3*A*). With the exception of a single cell (1 of 885), fixed-cell analysis revealed that the interphase PF16-depleted cells had typical polarity and cytoskeletal organization. However, 11.5% of the KD cells had four or more nuclei compared with only 1.2% in the control, suggesting impaired cytokinesis. These cells were categorized based on furrow progression; compared with the control, we observed an increase in cells that did not initiate a furrow or were in the process of cytokinesis or abscission. These data indicate a requirement of flagella function for *Giardia* cytokinesis (Fig. 2 *A* and *B*).

To explore the roles that PF16 and flagellar movement play in cytokinesis, we used DIC optics to film PF16-depleted cells between 16 and 28 h after morpholino treatment. Significant differences were observed between control and PF16-HA–KD cells in time taken to and ability to divide; statistical significance was verified by Kaplan–Meier survival analysis (Fig. 2 *C* and *D* and Fig. S4). To determine how PF16 impacts cleavage furrow ingression dynamics, we measured furrow progression from time-lapse movies of PF16-depleted cells. Because of varying levels of morpholino penetrance within the cell population, we examined the 11 slowest-dividing cells to identify the point at which these cells slowed or stalled their furrow progression. Consistent with an increase in the number of cells that did not initiate a furrow in the fixed-cell analysis, we found during live-cell analysis that, upon the onset of cytokinesis, furrow progression halted and did not reach the abscission stage (Fig. 2*E*, Fig. S3*B*, and Movie S4). In contrast, analysis of the 11 slowest control cells (lagging tail with division times >2 min) showed that the cleavage furrow rapidly proceeded to ~8 μm, experienced a short delay, and then completed division (Fig. 2*E*). These results indicate that the flagella are required to initiate cytokinesis. Given that the flagella are *Giardia's* only means for motility, it follows that the observed flexion of the intracytoplasmic axonemes of the caudal flagella initiate cell separation (Fig. 1 and Movies S1 and S2). As the daughter cells move apart, they become oriented such that beating of the extracellular flagella can propel the cells in opposite directions for scission. A mechanical role for the flagella, however, does not exclude the possibility that the flagella could have additional roles, such as serving as a scaffold for transport or polarity signaling (51, 60, 61).

Actin Has Two Major Roles for the Progression of Cytokinesis. We previously reported that actin depletion by morpholino KD results in the accumulation of aberrantly nucleated cells, indicating a role for actin in cytokinesis (31). However, our initial actin localization study reported actin localization in a cell that failed to complete cytokinesis and was not actively in the process of division (31).

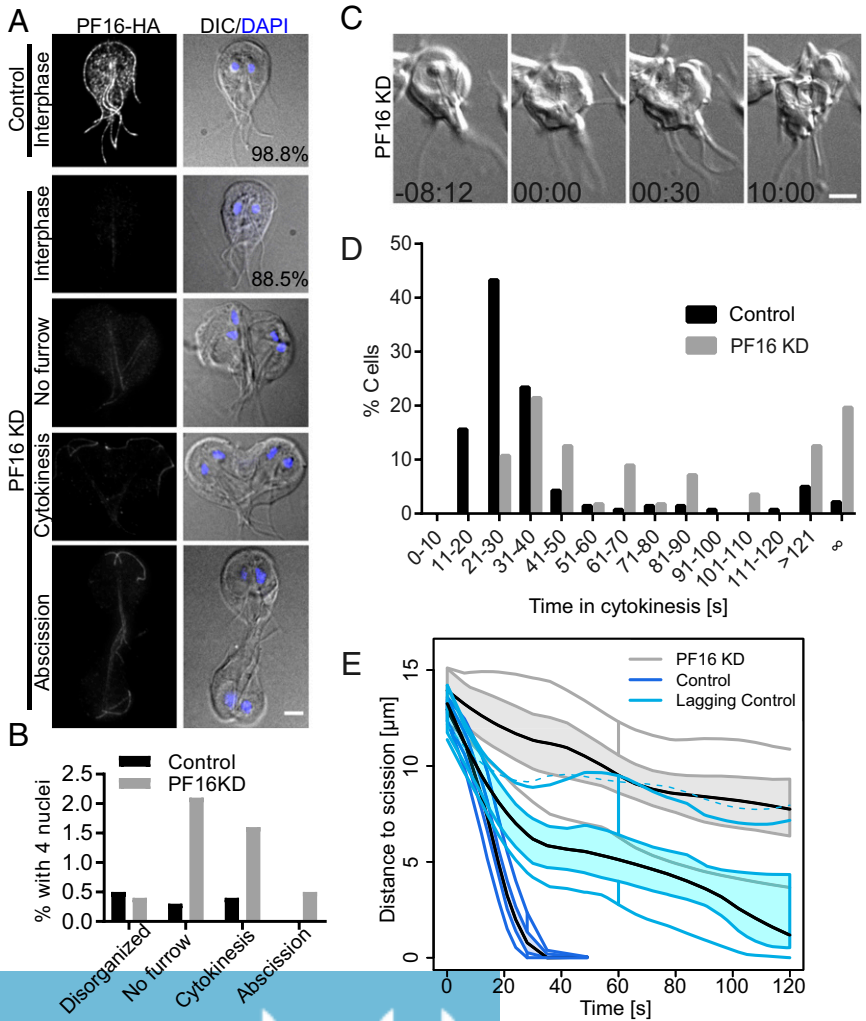

Fig. 2. Flagella function is required for furrowing progression and abscission. (*A*) PF16 localization in control and PF16-KD cells with equal exposure and scaling. Note that 98.8% of control and 88.5% of PF16-KD cells are normally organized interphase cells. (*B*) Categorization of the 1.2% of control and 11.5% of PF16 KD cells with four nuclei. With the exception of disorganized cells, which lacked normal polarity and could not be scored, images representing the categories are shown in *A*. (*C*) Still images from a time-lapse movie of a PF16-KD cell that failed to complete cytokinesis. (*D*) Histogram of division times for PF16-KD cells (n = 56) and morpholino control cells (n = 141). Data acquired from at least three independent replicates. (*E*) Functional box plot of furrow trajectories for the first 2 min of 11 PF16-KD cells that never completed cytokinesis (gray), compared with 20 randomly sampled control cells (blue) and the 11 slowest control cells (light blue). Central black line is the mean of the bootstrapped LOESS curves; the colored band indicates the 50% CI bound by 95% confidence bands of bootstrapped distances.

We therefore reexamined actin localization throughout the cell cycle (31). These studies were necessarily limited to fixed cells because attempts to fluorescently tag *Giardia* actin or to use common actin reporters have been unsuccessful in our hands. In agreement with our previous studies, actin was enriched around nuclei and forming spindles at the onset of mitosis, and remained enriched around the spindles and the developing axonemes throughout mitosis (Fig. 3*A*) (31, 62). The enrichment of actin around microtubule structures is consistent with actin's role in positioning them (31). We did not observe any actin structure that marked the position of the furrow, which is in contrast to cells with a contractile ring in which actin is enriched along the furrow. Actin levels were reduced in the first few microns of the cleavage furrow trajectory, and an actin clearing was regularly observed just ahead of the furrow cortex (Fig. 3*A*; see line scans across and through the furrow in Fig. S5). The actin cytoskeleton accounts for most of the mechanical properties of the cell cortex (63); thus, differential cortical reinforcement may indicate that selectively altering cortical mechanics is important for cleavage furrow ingression (18, 19).

To assess the role of actin during cytokinesis, we used time-lapse microscopy to image actin-depleted cells 16–26 h after morpholino treatment (Fig. 3*B*). Actin depletion significantly impacted division timing (Fig. S4). Actin-depleted cells fell into two distinct phenotypic classes: stalled cells, which took longer than 2 min to complete cytokinesis, and blocked cells, which never completed cytokinesis (Fig. 3 *B* and *C* and Movies S5 and S6). Some cells that never completed cytokinesis appeared to have mispositioned flagella that physically impeded cleavage furrow ingression (Fig. 3*B* and Movie S5). We previously reported that 40% of actin-depleted cells had mispositioned flagella 24 h after KD (31); we now understand that this could block cytokinesis through misdirected force generation or physically impeding the furrow. To further examine effects of actin KD on cleavage furrow ingression, we measured furrow progression in cells that were stalled in cytokinesis; we focused on those that took 6–15 min to complete cytokinesis, as this group was unique to the actin-depleted population. Furrow progression began at rates similar to control cells, but, after ~20 s, the rate of progression slowed (Fig. 3*D* and Fig. S3*D*). The cells were further delayed at the tail-to-tail stage, revealing that actin has a specific role in supporting the abscission step of cytokinesis. Slower progression could result from defects in cortical mechanics that may normally work to direct furrowing between the daughter cells. Considering that *Giardia* actin has an established role in trafficking (31), the stalled phenotype could also indicate a role for actin in coordinating membrane trafficking during cytokinesis.

Membrane Trafficking Is Essential for Cleavage Furrow Progression. In animals, plants, and fungi, tethering complexes target Golgi-derived vesicles to the plasma membrane to support the increase

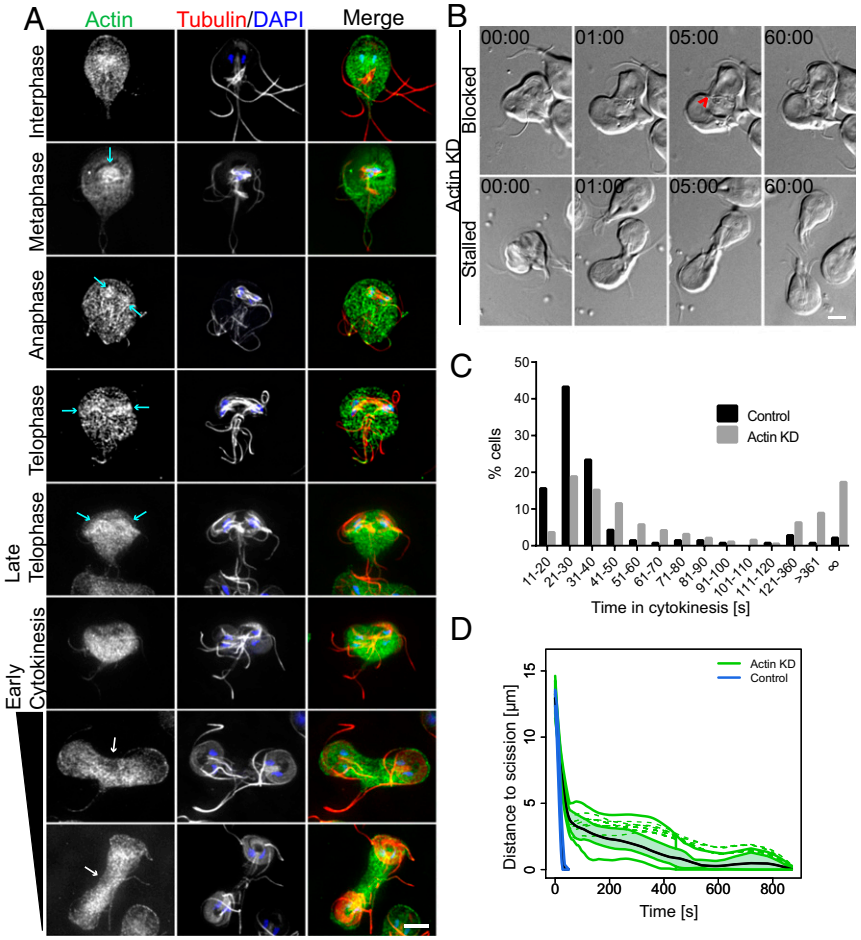

Fig. 3. Actin is required for abscission. (*A*) Immunofluorescence localization of Actin (green), tubulin (red), and DNA (blue) throughout the cell cycle. Actin accumulated around spindles and developed daughter ventral discs (cyan arrows). During cytokinesis, actin is found at relatively lower levels at the leading edge of the cleavage furrow (white arrows; analysis in Fig. S5). (*B*) Live cell imaging of actin KD reveals blocked and stalled cell phenotypes. Block of cytokinesis resulted from a flagella crossing the cleavage furrow path (red arrowhead; Movie S5). The stalled cell completes cytokinesis after ~60 min (Movie S6; time stamp, min:s). (Scale bars: 5 μm.) (*C*) Histogram of time to complete cytokinesis. Actin-KD cells (n = 191) take longer to divide than cells treated with the morpholino control (n =141). Data acquired from at least three independent experiments. (*D*) Functional box plot of bootstrapped LOESS curves for actin-KD cells (green, n = 12) taking 6–15 min to divide compared with typical control cells (blue, n = 20) shows a delay in abscission.

in surface area required for cytokinesis (64–66). In Fig. 1, we pointed out the ventrolateral flange, a lamellipodia-like membrane protrusion that is consumed during cytokinesis; this structure may serve as a source of plasma membrane (also see Movie S2). The rapid speed at which *Giardia* divides, the presence of a potential plasma membrane reservoir, and the lack of the exocyst and TRAPP-II tethering complexes (67), led us to question whether there is a requirement for new membrane delivery during cytokinesis. To address this, and generally disrupt endomembrane trafficking, we treated cells with Brefeldin A (BFA). BFA has been shown to disrupt endoplasmic reticulum (ER)-to-Golgi transport and change the distribution of membrane pools in model eukaryotes (68–70). Although *Giardia* lacks a conventional Golgi, BFA has been shown to potently disrupt trafficking out of the ER as well as disrupt COP1 localization (70–73), similar to plants and animals. As expected, BFA treatment induced swelling of the perinuclear ER, as visualized by the ER marker PDI2 (Fig. S3*E*) (74). BFA treatment similarly altered organization of the trafficking regulator Rab11, which has partially overlapping localization with PDI2 (Fig. S3*E*) and is required for cytokinesis in other eukaryotes (discussed later). Time-lapse microscopy and quantitative analyses revealed that BFA-treated cells completed cytokinesis at statistically slower rates or arrested with partially ingressed cleavage furrows (Fig. 4 *A* and *B* and Movie S7). To determine the point at which the treatment impacted furrow progression, we measured the distance to scission in cells that never completed cytokinesis. At the onset of cytokinesis, furrows are ∼14 μm long; BFA treatment stopped furrow progression shortly after cytokinesis began, with ∼8 μm of the furrow path remaining (Fig. 4*C* and Fig. S3*F*). This result demonstrates that impaired membrane trafficking blocks cytokinesis and may indicate a requirement for additional membrane and associated regulator factors in supporting cytokinesis.

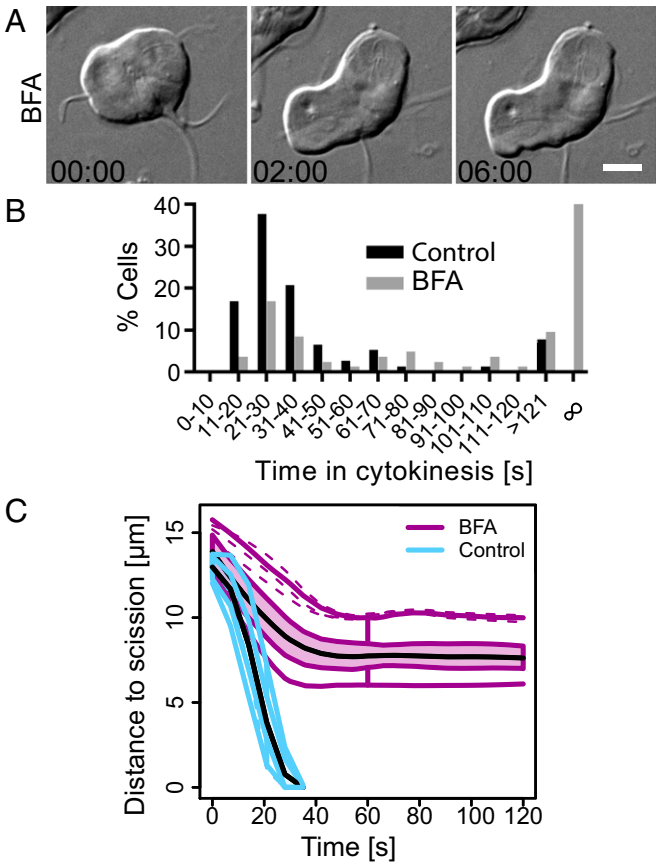

Fig. 4. Membrane partitioning is essential for cytokinesis. (*A*) Time-lapse images of a representative BFA-treated cell attempting cytokinesis. Note that furrow ingression consistently stops shortly after the start of cytokinesis (Movie S5). (Scale bar: 5 μm.) (*B*) Histogram of cytokinesis timing for BFA-treated (25 μM, $n = 83$) and control cells (0.35% DMSO, $n = 106$). Data for BFA acquired from three independent movies, data for DMSO control from two independent movies. (*C*) Functional box plot of bootstrapped LOESS curves for furrow ingression measurements of BFA-treated (pink, $n = 12$) and control cells (blue, $n = 12$).

Rab11-GTPase Localizes to the Prefurrow and Is Necessary for Cytokinesis. Rab11 is essential for delivering membrane and cytoskeletal effector proteins to the cleavage furrow in plants, animals, and the protist *T. brucei* (75–78). In animal cells, Rab11 is further used to support abscission via plus-end trafficking on microtubules of the midbody (65, 76). We used live-cell imaging to localize Rab11 throughout the cell cycle. In interphase cells, mNG-C18-Rab11 (mNG-Rab11) localized to the perinuclear ER and cell cortex (Fig. 5*A*). In late telophase, bright puncta and linear arrays of mNG-Rab11 were observed that corresponded to the position of intracytoplasmic axonemes ($n = 20$ cells; Fig. 5*A* and Movie S8). Fixed-cell analysis confirmed that the linear arrays are aligned with intracellular axonemes, implicating the flagella as highways for vesicle transport (Fig. 5*B*). Ahead of anterior-to-posterior furrow ingression, Rab11 transiently delineated the cleavage furrow, indicating a role in prefurrowing. Prefurrowing (i.e., formation of a dorsal-ventral invagination) could be observed in 4D DIC movies to occur 13.4 ± 5 s ($n = 50$ cells) ahead of anterior-posterior furrow progression. As the anterior-posterior furrow advanced, mNG-Rab11 remained at the leading edge of the cleavage furrow, as well as along the length of the furrow (Fig. 5*A* and Movie S8). Remarkably, fixed-cell analysis revealed that, in addition to loading onto the intracytoplasmic axonemes of mature flagella, Rab11 was concentrated at the ends of the developing axonemes positioned to traffic Rab11 directly into the furrow (Fig. 5*B* and Movie S9). Similarly oriented to midbody microtubules, the plus ends of these axonemes terminate at the future site of the furrow; we propose that these developing axonemes have analogous function to the midbody/phragmoplast and are used to guide trafficking into the furrow. Consistent with a role for actin in supporting vesicular trafficking, actin was observed to colocalize with Rab11 near the ends of the growing flagella tips (Fig. 5*B*, Fig. S6*A*, and Movie S9).

To verify a functional role for Rab11 in *Giardia* cytokinesis, we depleted Rab11 with morpholinos and validated the KD by generating an endogenously tagged morpholino-sensitive (79) HA-Rab11 cell line. At 24 h after electroporation, Rab11 was depleted by ∼70% vs. the control (Fig. S6*E*). Rab11-depleted cells took longer to divide or failed to divide, in agreement with a critical contribution of membrane remodeling toward cleavage furrow progression, consistent with the phenotype produced by dominant-negative and constitutively active Rab11 mutants (Fig. 5 *C* and *D* and Figs. S4 and S6). The *Giardia* genome contains six Rab proteins. The more severe impairment of cytokinesis by BFA treatment may indicate that Rab11 accounts for only a subset of the membrane remodeling associated with cytokinesis. However, the overall importance of Rab11 for cytokinesis is likely underreported by our timing data, as many cells that completed division with normal kinetics had abnormal cleavage furrow placement or generated daughter cells with irregular morphology, reminiscent of the actin KD phenotype. Importantly, conservation of Rab11 function in *Giardia* implicates Rab11 as an ancient component of the cell division machinery.

Colocalization between Rab11 and actin, as well as the abscission defect associated with depletion of either protein, suggests that these two systems act cooperatively. Thus, we examined whether Rab11 localization was impacted by actin KD. In addition to cells with abnormally positioned flagella, which could alter Rab11 trafficking, we observed that 55% of cells had abnormal morphology at the abscission site compared with 14% in the controls (Fig. 5 *E* and *F*). This defect included missing regions of the cell body and/or Rab11-positive membrane accumulation at the abscission site. During DIC imaging of control cells, similar membrane accumulations were sometimes observed to form after abscission, particularly for cells initially connected by a cytoplasmic

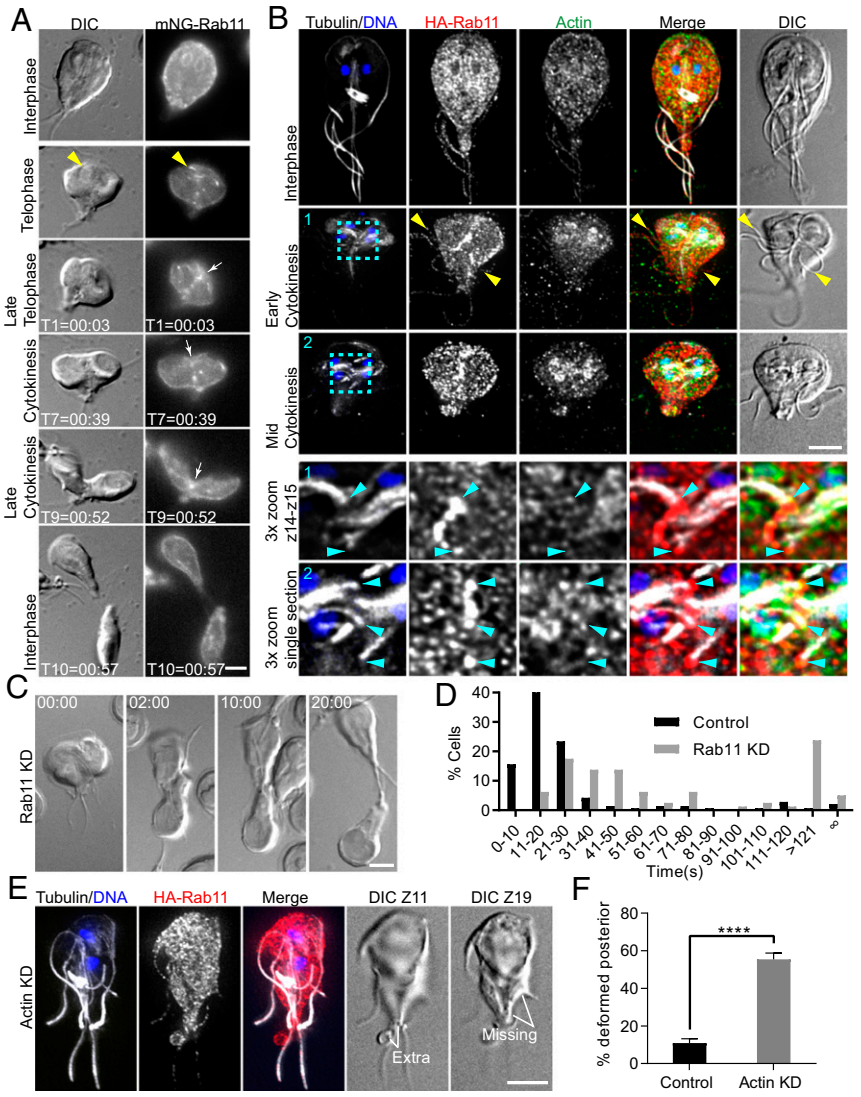

Fig. 5. Rab11 traffics to the furrow on flagella and is required for abscission. (*A*) mNG-Rab11 localization through the cell cycle. In late telophase, Rab11 is recruited to intracytoplasmic axonemes (yellow arrowhead), and, immediately before anterior-posterior furrow ingression, Rab11 delineates the furrow (white arrow). mNG-Rab11 remained in the cleavage furrow and at the leading edge of the advancing furrow during cytokinesis (white arrow; time stamp, min:s). (*B*) Immunofluorescence localization of tubulin (grayscale), actin (green), HA-Rab11 (red), and DNA (blue). HA-Rab11 localized to the ER in interphase cells. During late telophase, Rab11 loaded onto flagella (yellow arrowheads). Just ahead of anterior-to-posterior furrow progression, HA-Rab11 accumulated in the furrow. Enlarged images correspond to cyan boxes with two or one optical section that show Rab11 and actin accumulating at the ends of the nascent flagella (blue arrowheads). (*C*) Rab11 antisense morpholino-treated cells are delayed in abscission and frequently have abnormal furrow positioning. (*D*) Histogram of division timing for Rab11 KD ($n = 80$) and morpholino control ($n = 141$). (*E*) Example of an actin-KD cell with abnormal posterior morphology and a membrane accumulation. (*F*) Quantification of this phenotype for actin depleted ($n = 602$) and morpholino control cells ($n = 613$). (Scale bars: 5 μm.)

bridge. The excess membrane was eventually retracted and incorporated into the cell body, but actin-depleted cells often had thicker than usual cytoplasmic bridges, which could account for the excessive membrane found at the abscission site. The abnormal abscission site morphology and increased number of cells with Rab11-labeled membrane accumulations is consistent with actin coordinating the final membrane-remodeling steps required for abscission.

Discussion

Here, we set out to study how *Giardia*, a highly divergent eukaryote, lacking the conserved contractile ring and amoeboid motility proteins, carries out cell division. By using newly developed live-cell imaging methodologies, genetic disruption, and drug studies, we have established a role for membrane trafficking and the cytoskeleton in *Giardia* cytokinesis, as well as revealing several twists on extant mechanistic themes. Within *Giardia's* 8-h cell cycle, a relatively brief period is spent in mitosis and cytokinesis. For fixed-cell studies of nonsynchronized cells, our results indicate that only approximately 1.3% of the cells will be in mitosis (6.5 min of 8 h) and 0.17% of the cells will be in cytokinesis (50 s of 8 h). These percentages are in agreement with the previously reported mitotic index (30). However, in the past, challenges associated with finding and staging rarely observed dividing *Giardia* led to a misunderstanding of the normal progression of mitosis and cytokinesis. Cells in the process of cytokinesis should have daughter cells smaller than interphase trophozoites, lacking a median body, and possessing only four full-length flagella. The often-shown heart-shaped cells with daughter cells equivalent in size to interphase trophozoites are abnormal cells that failed to complete cytokinesis. These are the ~1% of cells that never completed cytokinesis in our controls

(Fig. S1*C*). Remarkably, we observed heart-shaped cells recovering in the next round of division. We and others have mistakenly interpreted these configurations to be in the process of cytokinesis when they were not actively dividing (25, 30, 31, 80–82). Therefore, the methodical advances and observations described here are of immense value for understanding the process of cytokinesis and enabling additional studies of living and dividing *Giardia*. Importantly, unique and divergent molecular machinery in *Giardia* has the potential to be leveraged for the treatment of this major parasite. In particular, *Giardia*-specific proteins that regulate cell polarity and coordinate the cytoskeletal dynamics and membrane remodeling described here could be important therapeutic targets for clearing infection (4).

The Inside-Out Model for *Giardia* Cytokinesis. Based on our analyses, we present a working model that can explain myosin-independent cytokinesis in *Giardia* (Fig. 6). Upon initiation of mitosis, the basal bodies and anterior flagellar exit sites are repositioned in a process that is, in part, actin-dependent (Figs. 1 and 3) (31). The microtubules used to form the two spindles are derived from the median body (Fig. 1). At the end of mitosis, the two spindles transition from cage-like to bundled organization. The two daughter discs and four nascent flagella are assembled in opposing orientations near the spindle poles. As the daughter discs are further developed, the parental disk thins out; disassembly of the overlap zone of the disk coincides with the start of cytokinesis. The tips of the depolymerizing parental disk were sometimes observed to be coated with Rab11; thus, the disk may act as the initial guide for Rab11 enrichment between daughter cells. Force generated by the internal axonemes of the caudal flagella drive the daughter cells in opposite directions. This movement causes the plasma membrane to stretch around the two daughter discs, leading to membrane tension (Fig. 1 and Movies S1–S3). Actin is cleared just ahead of the furrow cortex and may act to direct the progression of the cleavage furrow (Fig. S5). Additional membrane delivery is mediated by Rab11 vesicles that are trafficked along the intracytoplasmic axonemes and ultimately delivered by the growing posterolateral and ventral flagella, whose plus ends point toward the furrow and act as the functional equivalent of a midbody/phragmoplast (Fig. 5). Just before scission, the force for daughter cell separation transitions from flexion of the intracytoplasmic caudal flagella axonemes to propulsion by the beating external portions of the flagella, driving the cells in opposite directions (Movies S1–S3). The final swimming stage is reminiscent of traction-mediated cytokinesis observed in myosin II mutants of other eukaryotes; here swimming, rather than crawling, provides the force to pull the daughter cells apart.

An emerging view is that flagella may play a fundamental role in protozoan cytokinesis. In addition to a role in force generation, flagella act as scaffolds for signaling and polarity (51, 60, 61). A requirement for motility in abscission has previously been reported for *T. brucei*, a protist that also lacks an actomyosin-based cytokinetic apparatus (51, 52, 83, 84), and *Tetrahymena thermophila*, which uses ciliary-driven cell motility during cytokinesis (50, 85, 86). In *T. brucei*, more than 30 different motility mutants have been reported to have cell-separation defects that correlate with the motility defect (2). Remarkably, abscission defects can be rescued by mechanical agitation, illustrating the importance of membrane tension for abscission (52, 84). Given the large number of protists that lack myosin II (20, 21), a role for flagella in cytokinesis could be more common in nature than what is presumed from studies of model eukaryotes, which represent only a small proportion of the eukaryotic tree.

Instead of Taking the Lead, Actin Plays a Supporting Role in Furrowing. Given actin's central role in cell division of model eukaryotes, it is not surprising that actin has a role in *Giardia*'s cytokinesis, yet the implementation is different. Distinct from that observed in model eukaryotes, *Giardia* actin is notably found at high levels along the cell edges where the ventral disk presses against the plasma membrane, but is cleared just ahead of the advancing furrow

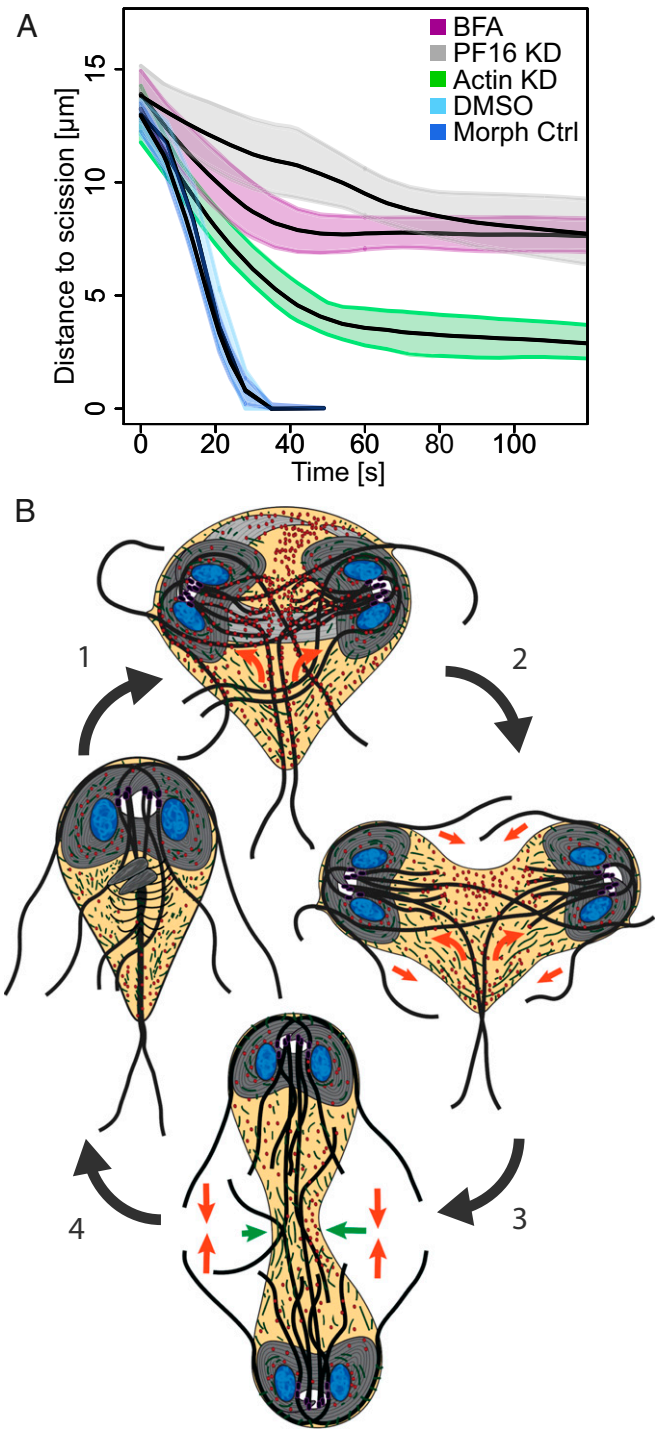

Fig. 6. Model for cytokinesis in *Giardia*. (*A*) Comparison of experimental perturbations and their corresponding control treatments. Note the distance to scission at which each perturbed cellular system slowed or arrested division. The stall point is interpreted as the point at which the pathway contributes to furrow progression. (*B*) Model for myosin-independent cytokinesis. The ventral discs in gray, actin in green, Rab11 in red, and forces driving daughter cell separation are indicated by orange arrows. *1*, Mitosis is initiated, actin positions the microtubule cytoskeleton. *2*, Rab11 loads onto the intracytoplasmic axonemes and is guided into the furrow by the nascent axonemes. Ventral disk opening permits furrow progression, and the intracytoplasmic caudal flagella push daughter discs in opposite directions to initiate a furrow. *3*, Caudal axonemes continue pushing discs apart, and differential cortical actin and Laplace pressure (green arrows) direct furrow advancement. *4*, Flagella propulsion generates cortical tension between daughter cells and actin, and Rab11 coordinates membrane remodeling for abscission.

(Fig. S5). We propose that *Giardia* actin has a role in guiding cleavage furrow ingression. Cortical tension and membrane fluidity are important factors in regulating cytokinesis in model systems (18, 87). Abnormal furrow placement and delayed abscission resulting from actin depletion are consistent with this proposed role (Fig. 5 *E* and *F*). However, we propose that actin's most critical role is in positioning the tubulin cytoskeleton so that the flagella can direct trafficking and force generation along the furrow. The mechanism used to activate actin polymerization for organelle positioning and differential cortical organization remain to be determined, although it is likely that *Giardia's* sole Rho family GTPase, GlRac, has some role in coordinating actin polymerization and membrane remodeling during cytokinesis (31, 79).

In otherwise normal-looking cells, we observed many actin-depleted and Rab11-depleted cells that were stuck at the tail-to-tail stage of cytokinesis. This indicates a role for these proteins in the final membrane-remodeling events required for abscission. A subset of Rab11 vesicles colocalize with actin in interphase cells, and, in dividing cells, actin and Rab11 were observed to colocalize near the ends of the nascent flagella. This is consistent with actin having some role in directing Rab11 traffic. In other systems, Rab11 has been found to use dynein, kinesins, and myosins for transport when long-distance trafficking is supported by the microtubule cytoskeleton and actin is used for short-range transport. *Giardia* lacks all myosin homologs and the FIP proteins that normally connect Rab11 to molecular motors (88). Given localization of Rab11 to the flagella and tips of depolymerizing discs, it seems likely that dynein and kinesin motors are used to support Rab11 trafficking. The specific molecules that link Rab11 to the actin and tubulin cytoskeleton and whether GlRab11 delivers cytoskeletal effectors to the furrow as in animal cells (reviewed in ref. 65) remain to be determined.

Materials and Methods

Parasite Strain and Growth Conditions. G. *lamblia* strain WB clone 6 (ATCC 50803; American Type Culture Collection) was cultured as in a previous work (30).

Morpholino KD. KD experiments were performed as described previously (89) with morpholinos sourced from Gene Tools. Sequences are provided in Dataset S2.

Vector Construction. All constructs used in this study were made by using standard techniques. Dataset S2 provides sequences and workflow. Note that N-terminal fusions result in morpholino-resistant constructs (62), and therefore we included the first 27 bp of the coding sequence to restore morpholino sensitivity (79) to the 3HA-Rab11^{MS} construct.

Live Imaging. In an effort to increase the mitotic index, cells were treated with 0.25 μM albendazole ~4 h before being imaged. Cells were chilled with ice for 20 min to detach from the culture tube and then placed into an Attofluor cell chamber (Molecular Probes) and incubated in a GasPak EZ anaerobic pouch (BD) for 1–2 h at 37 °C. Cells were then washed four times with SB5050 (0.1% K_2HPO_4, 0.06% KH_2PO_4, 1% glucose, 0.2% NaCl, 0.2% cysteine-HCl monohydrate, 0.02% ascorbic acid, 0.0228% ferric ammonium citrate, 0.05% bovine bile, and 5% bovine serum, pH 7.1; see Dataset S1 for variants tested). Drug-free cells were overlaid with a mixture of 0.7–1% ultra-low gelling agarose (Sigma A2576) melted in Hepes-buffered saline (137 mM NaCl, 5 mM KCl, 0.91 mM Na_2HpO_4-heptahydrate, 5.55 mM glucose, 20 mM Hepes, pH 7) and diluted into SB5050 and left at room temperature for 10 min to solidify the agarose. Imaging was performed under 2.5% O_2, 5% CO_2, and 37 °C (Boldline CO_2/O_2; Oko Lab). Time-lapse imaging was performed on a DeltaVision Elite microscope (GE) equipped with DIC optics, using a 100 × 1.4 NA or 60 × 1.42 NA objective, and a sCMOS 5.4 PCIe air-cooled camera (PCO-TECH).

Long-Term Imaging with DIC. Cells were imaged as described earlier; however, cells were not exposed to albendazole, and the washes and overlay used standard TYDK media (90) instead of SB5050.

Cleavage Furrow Measurements. Measurements were made along the length of the cleavage furrow, anterior to posterior, starting on the onset of cytokinesis through the completion of the process, by using SoftWorx (API).

Cell Division Rate Assay. Confluent cultures were diluted by 60%. The cells were incubated in 50 ng/mL albendazole at 37 °C for 5.5 h. Cells were detached and collected by centrifugation. The cell pellet was resuspended in 6 mL drug-free media, and 1 mL of cell culture was mixed with paraformaldehyde and then counted on a hemocytometer. The remaining 5 mL cell culture was placed at 37 °C for 1 h and then fixed with paraformaldehyde and counted on a hemocytometer.

Immunofluorescence Microscopy. Fixed imaging was performed as in a previous work (79) using starve and release (3.5 h) to increase the mitotic index (30).

Western Blotting. Blotting was performed as in a previous work (89).

BFA Treatment. The long-term imaging with DIC as detailed earlier, except cells were exposed to 25 μM BFA in 0.035% DMSO 3 h before and during imaging.

Statistical Analysis. Highly statistically significant differences between times until cytokinesis are obtained by Kaplan–Meier estimator, a nonparametric method (i.e., does not require distributional assumptions) from survival analysis (91). We set a conservative censoring rule for cells that do not complete cytokinesis at 900 s without completion, a lower bound on widely varying total imaging times. To create curves and confidence bands, cleavage furrow measurements obtained at each frame of imaging data were interpolated by using local polynomial (i.e., LOESS) regression, producing a smooth curve corresponding to each representative cell (91). Resampling this set of curves with replacement to generate 5,000 bootstrap replicate datasets, we obtained nonparametric estimates of the median curve and 95% CIs (92). These results are displayed by using standard pointwise confidence bands as well as using functional box plots for completeness, which generalize notions such as outliers to entire curves rather than points (detailed in ref. 93). In this case, the two visualization methods are not noticeably different, and provide more detailed support for results of formal hypothesis tests of significance based on Kaplan–Meier estimates of time until cytokinesis. Plots were generated by using R (www.R-project.org).

ACKNOWLEDGMENTS. The authors thank B. Wakimoto, S. Parkhurst, C. Asbury, L. Wordeman, and J. Vicente for critical reading of the manuscript and E. Thomas, M. Steele-Ogus, and K. Hennessey for help with editing. This work was supported by National Institutes of Health Grant 5R01AI110708 (to A.R.P.) and National Science Foundation Grant GRFP DGE-1256082 (to W.R.H.).

1. Vermeulen K, Van Bockstaele DR, Berneman ZN (2003) The cell cycle: A review of regulation, deregulation and therapeutic targets in cancer. *Cell Prolif* 36:131–149.
2. Ralston KS, Hill KL (2008) The flagellum of Trypanosoma brucei: New tricks from an old dog. *Int J Parasitol* 38:869–884.
3. Lock RL, Harry EJ (2008) Cell-division inhibitors: New insights for future antibiotics. *Nat Rev Drug Discov* 7:324–338.
4. Hennessey KM, et al. (2016) Identification and validation of small-gatekeeper kinases as drug targets in Giardia lamblia. *PLoS Negl Trop Dis* 10:e0005107.
5. Lane S, Lloyd D (2002) Current trends in research into the waterborne parasite Giardia. *Crit Rev Microbiol* 28:123–147.
6. Baldauf SL (2003) The deep roots of eukaryotes. *Science* 300:1703–1706.
7. He D, et al. (2014) An alternative root for the eukaryote tree of life. *Curr Biol* 24:465–470.
8. Dawson SC, Paredez AR (2013) Alternative cytoskeletal landscapes: Cytoskeletal novelty and evolution in basal excavate protists. *Curr Opin Cell Biol* 25:134–141.
9. Fritz-Laylin LK, et al. (2010) The genome of Naegleria gruberi illuminates early eukaryotic versatility. *Cell* 140:631–642.
10. Hampl V, et al. (2009) Phylogenomic analyses support the monophyly of Excavata and resolve relationships among eukaryotic "supergroups". *Proc Natl Acad Sci USA* 106:3859–3864.
11. D'Avino PP, Giansanti MG, Petronczki M (2015) Cytokinesis in animal cells. *Cold Spring Harb Perspect Biol* 7:a015834.
12. Guizetti J, Gerlich DW (2012) ESCRT-III polymers in membrane neck constriction. *Trends Cell Biol* 22:133–140.
13. Müller S, Jürgens G (2016) Plant cytokinesis-No ring, no constriction but centrifugal construction of the partitioning membrane. *Semin Cell Dev Biol* 53:10–18.
14. Baluska F, Menzel D, Barlow PW (2006) Cytokinesis in plant and animal cells: Endosomes 'shut the door'. *Dev Biol* 294:1–10.
15. Kanada M, Nagasaki A, Uyeda TQP (2005) Adhesion-dependent and contractile ring-independent equatorial furrowing during cytokinesis in mammalian cells. *Mol Biol Cell* 16:3865–3872.
16. Uyeda TQP, Kitayama C, Yumura S (2000) Myosin II-independent cytokinesis in Dictyostelium: Its mechanism and implications. *Cell Struct Funct* 25:1–10.
17. Neujahr R, Heizer C, Gerisch G (1997) Myosin II-independent processes in mitotic cells of Dictyostelium discoideum: Redistribution of the nuclei, re-arrangement of the actin system and formation of the cleavage furrow. *J Cell Sci* 110:123–137.
18. Poirier CC, Ng WP, Robinson DN, Iglesias PA (2012) Deconvolution of the cellular force-generating subsystems that govern cytokinesis furrow ingression. *PLOS Comput Biol* 8:e1002467.

19. Zhang W, Robinson DN (2005) Balance of actively generated contractile and resistive forces controls cytokinesis dynamics. *Proc Natl Acad Sci USA* 102:7186–7191.
20. Foth BJ, Goedecke MC, Soldati D (2006) New insights into myosin evolution and classification. *Proc Natl Acad Sci USA* 103:3681–3686.
21. Sebé-Pedrós A, Grau-Bové X, Richards TA, Ruiz-Trillo I (2014) Evolution and classification of myosins, a paneukaryotic whole-genome approach. *Genome Biol Evol* 6:290–305.
22. Eggert US, Mitchison TJ, Field CM (2006) Animal cytokinesis: From parts list to mechanisms. *Annu Rev Biochem* 75:543–566.
23. Pollard TD, Wu JQ (2010) Understanding cytokinesis: Lessons from fission yeast. *Nat Rev Mol Cell Biol* 11:149–155.
24. Gut J, et al. (2011) An image-based assay for high throughput screening of Giardia lamblia. *J Microbiol Methods* 84:398–405.
25. Benchimol M (2004) Mitosis in Giardia lamblia: Multiple modes of cytokinesis. *Protist* 155:33–44.
26. Ghosh S, Frisardi M, Rogers R, Samuelson J (2001) How Giardia swim and divide. *Infect Immun* 69:7866–7872.
27. Kabnick KS, Peattie DA (1990) In situ analyses reveal that the two nuclei of Giardia lamblia are equivalent. *J Cell Sci* 95:353–360.
28. Solari AJ, Rahn MI, Saura A, Lujan HD (2003) A Unique mechanism of nuclear division in Giardia lamblia involves components of the ventral disk and the nuclear envelope. *Biocell* 27:329–346.
29. Yu LZ, Birky CW, Jr, Adam RD (2002) The two nuclei of Giardia each have complete copies of the genome and are partitioned equationally at cytokinesis. *Eukaryot Cell* 1:191–199.
30. Sagolla MS, Dawson SC, Mancuso JJ, Cande WZ (2006) Three-dimensional analysis of mitosis and cytokinesis in the binucleate parasite Giardia intestinalis. *J Cell Sci* 119:4889–4900.
31. Paredez AR, et al. (2011) An actin cytoskeleton with evolutionarily conserved functions in the absence of canonical actin-binding proteins. *Proc Natl Acad Sci USA* 108:6151–6156.
32. Tůmová P, Kulda J, Nohýnková E (2007) Cell division of Giardia intestinalis: Assembly and disassembly of the adhesive disc, and the cytokinesis. *Cell Motil Cytoskeleton* 64:288–298.
33. Shaner NC, et al. (2013) A bright monomeric green fluorescent protein derived from Branchiostoma lanceolatum. *Nat Methods* 10:407–409.
34. Cheffings TH, Burroughs NJ, Balasubramanian MK (2016) Actomyosin ring formation and tension generation in eukaryotic cytokinesis. *Curr Biol* 26:R719–R737.
35. Dawson SC, House SA (2010) Imaging and analysis of the microtubule cytoskeleton in Giardia. *Methods Cell Biol* 97:307–339.
36. Crossley R, Marshall J, Clark JT, Holberton DV (1986) Immunocytochemical differentiation of microtubules in the cytoskeleton of Giardia lamblia using monoclonal antibodies to alpha-tubulin and polyclonal antibodies to associated low molecular weight proteins. *J Cell Sci* 80:233–252.
37. Feely DEEDV (1990) The Biology of Giardia. *Giardiasis*, ed Mayer EA (Elsevier, Amsterdam), pp 11–49.
38. Morrison HG, et al. (2007) Genomic minimalism in the early diverging intestinal parasite Giardia lamblia. *Science* 317:1921–1926.
39. Lenaghan SC, Davis CA, Henson WR, Zhang Z, Zhang M (2011) High-speed microscopic imaging of flagella motility and swimming in Giardia lamblia trophozoites. *Proc Natl Acad Sci USA* 108:E550–E558.
40. McInally SG, Dawson SC (2016) Eight unique basal bodies in the multi-flagellated diplomonad Giardia lamblia. *Cilia* 5:21.
41. House SA, Richter DJ, Pham JK, Dawson SC (2011) Giardia flagellar motility is not directly required to maintain attachment to surfaces. *PLoS Pathog* 7:e1002167.
42. Ludington WB, Shi LZ, Zhu Q, Berns MW, Marshall WF (2012) Organelle size equalization by a constitutive process. *Curr Biol* 22:2173–2179.
43. Nohynková E, Tumová P, Kulda J (2006) Cell division of Giardia intestinalis: Flagellar developmental cycle involves transformation and exchange of flagella between mastigonts of a diplomonad cell. *Eukaryot Cell* 5:753–761.
44. Vicente JJ, Cande WZ (2014) Mad2, Bub3, and Mps1 regulate chromosome segregation and mitotic synchrony in Giardia intestinalis, a binucleateprotist lacking an anaphase-promoting complex. *Mol Biol Cell* 25:2774–2787.
45. Azimzadeh J, Traas J, Pastuglia M (2001) Molecular aspects of microtubule dynamics in plants. *Curr Opin Plant Biol* 4:513–519.
46. Kumagai F, et al. (2001) Fate of nascent microtubules organized at the M/G1 interface, as visualized by synchronized tobacco BY-2 cells stably expressing GFP-tubulin: Time-sequence observations of the reorganization of cortical microtubules in living plant cells. *Plant Cell Physiol* 42:723–732.
47. Mullins JM, Biesele JJ (1977) Terminal phase of cytokinesis in D-98s cells. *J Cell Biol* 73: 672–684.
48. Nagasaki A, de Hostos EL, Uyeda TQ (2002) Genetic and morphological evidence for two parallel pathways of cell-cycle-coupled cytokinesis in Dictyostelium. *J Cell Sci* 115:2241–2251.
49. Hahn J, et al. (2013) High sensitivity of Giardia duodenalis to tetrahydrolipstatin (orlistat) in vitro. *PLoS One* 8:e71597.
50. Brown JM, Hardin C, Gaertig J (1999) Rotokinesis, a novel phenomenon of cell locomotion-assisted cytokinesis in the ciliate Tetrahymena thermophila. *Cell Biol Int* 23:841–848.
51. Langousis G, Hill KL (2014) Motility and more: The flagellum of Trypanosomabrucei. *Nat Rev Microbiol* 12:505–518.
52. Ralston KS, Lerner AG, Diener DR, Hill KL (2006) Flagellar motility contributes to cytokinesis in Trypanosoma brucei and is modulated by an evolutionarily conserved dynein regulatory system. *Eukaryot Cell* 5:696–711.
53. Engel BD, et al. (2011) A cell-based screen for inhibitors of flagella-driven motility in Chlamydomonas reveals a novel modulator of ciliary length and retrograde actin flow. *Cytoskeleton* 68:188–203.
54. Firestone AJ, et al. (2012) Small-molecule inhibitors of the AAA+ ATPase motor cytoplasmic dynein. *Nature* 484:125–129.
55. Wada Y, Baba SA, Kamimura S (2015) Effects of the dynein inhibitor ciliobrevin on the flagellar motility of sea urchin spermatozoa. *Cytoskeleton* 72:182–192.
56. Smith EF, Lefebvre PA (1996) PF16 encodes a protein with armadillo repeats and localizes to a single microtubule of the central apparatus in Chlamydomonas flagella. *J Cell Biol* 132:359–370.
57. Dutcher SK, Huang B, Luck DJ (1984) Genetic dissection of the central pair microtubules of the flagella of Chlamydomonas reinhardtii. *J Cell Biol* 98:229–236.
58. Sapiro R, et al. (2002) Male infertility, impaired sperm motility, and hydrocephalus in mice deficient in sperm-associated antigen 6. *Mol Cell Biol* 22:6298–6305.
59. Gourguechon S, Cande WZ (2011) Rapid tagging and integration of genes in Giardia intestinalis. *Eukaryot Cell* 10:142–145.
60. de Graffenried CL, Ho HH, Warren G (2008) Polo-like kinase is required for Golgi and bilobe biogenesis in Trypanosoma brucei. *J Cell Biol* 181:431–438.
61. Li Z, Umeyama T, Li Z, Wang CC (2010) Polo-like kinase guides cytokinesis in Trypanosoma brucei through an indirect means. *Eukaryot Cell* 9:705–716.
62. Paredez AR, Nayeri A, Xu JW, Krtková J, Cande WZ (2014) Identification of obscure yet conserved actin-associated proteins in Giardia lamblia. *Eukaryot Cell* 13:776–784.
63. Girard KD, Chaney C, Delannoy M, Kuo SC, Robinson DN (2004) Dynacortin contributes to cortical viscoelasticity and helps define the shape changes of cytokinesis. *EMBO J* 23:1536–1546.
64. Rybak K, et al. (2014) Plant cytokinesis is orchestrated by the sequential action of the TRAPPII and exocyst tethering complexes. *Dev Cell* 29:607–620.
65. Schiel JA, Childs C, Prekeris R (2013) Endocytic transport and cytokinesis: From regulation of the cytoskeleton to midbody inheritance. *Trends Cell Biol* 23:319–327.
66. Wang N, Lee IJ, Rask G, Wu JQ (2016) Roles of the TRAPP-II complex and the exocyst in membrane deposition during fission yeast cytokinesis. *PLoS Biol* 14:e1002437.
67. Koumandou VL, Dacks JB, Coulson RM, Field MC (2007) Control systems for membrane fusion in the ancestral eukaryote; evolution of tethering complexes and SM proteins. *BMC EvolBiol* 7:29.
68. Donaldson JG, Finazzi D, Klausner RD (1992) Brefeldin A inhibits Golgi membrane-catalysed exchange of guanine nucleotide onto ARF protein. *Nature* 360:350–352.
69. Helms JB, Rothman JE (1992) Inhibition by Brefeldin A of a Golgi membrane enzyme that catalyses exchange of guanine nucleotide bound to ARF. *Nature* 360:352–354.
70. Ritzenthaler C, et al. (2002) Reevaluation of the effects of brefeldinA on plant cells using tobacco Bright Yellow 2 cells expressing Golgi-targeted green fluorescent protein and COPI antisera. *Plant Cell* 14:237–261.
71. Stefanic S, et al. (2009) Neogenesis and maturation of transient Golgi-like cisternae in a simple eukaryote. *J Cell Sci* 122:2846–2856.
72. Luján HD, et al. (1995) Developmental induction of Golgi structure and function in the primitive eukaryote Giardia lamblia. *J Biol Chem* 270:4612–4618.
73. Touz MC, Kulakova L, Nash TE (2004) Adaptor protein complex 1 mediates the transport of lysosomal proteins from a Golgi-like organelle to peripheral vacuoles in the primitive eukaryote Giardia lamblia. *Mol Biol Cell* 15:3053–3060.
74. Abodeely M, et al. (2009) A contiguous compartment functions as endoplasmic reticulum and endosome/lysosome in Giardia lamblia. *Eukaryot Cell* 8:1665–1676.
75. Fielding AB, et al. (2005) Rab11-FIP3 and FIP4 interact with Arf6 and the exocyst to control membrane traffic in cytokinesis. *EMBO J* 24:3389–3399.
76. Wilson GM, et al. (2005) The FIP3-Rab11 protein complex regulates recycling endosome targeting to the cleavage furrow during late cytokinesis. *Mol Biol Cell* 16:849–860.
77. Chow CM, Neto H, Foucart C, Moore I (2008) Rab-A2 and Rab-A3 GTPases define a trans-Golgi endosomal membrane domain in Arabidopsis that contributes substantially to the cell plate. *Plant Cell* 20:101–123.
78. Gabernet-Castello C, Dubois KN, Nimmo C, Field MC (2011) Rab11 function in Trypanosoma brucei: Identification of conserved and novel interaction partners. *Eukaryot Cell* 10:1082–1094.
79. Krtková J, et al. (2016) Rac regulates Giardia lamblia encystation by coordinating cyst wall protein trafficking and secretion. *MBio* 7:e01003-16.
80. Dunn LA, et al. (2007) The activity of protease inhibitors against Giardia duodenalis and metronidazole-resistant Trichomonas vaginalis. *Int J Antimicrob Agents* 29:98–102.
81. Benchimol M (2004) Participation of the adhesive disc during karyokinesis in Giardia lamblia. *Biol Cell* 96:291–301.
82. Piva B, Benchimol M (2004) The median body of Giardia lamblia: An ultrastructural study. *Biol Cell* 96:735–746.
83. García-Salcedo JA, et al. (2004) A differential role for actin during the life cycle of Trypanosoma brucei. *EMBO J* 23:780–789.
84. Branche C, et al. (2006) Conserved and specific functions of axoneme components in trypanosome motility. *J Cell Sci* 119:3443–3455.
85. Brown JM, Marsala C, Kosoy R, Gaertig J (1999) Kinesin-II is preferentially targeted to assembling cilia and is required for ciliogenesis and normal cytokinesis in Tetrahymena. *Mol Biol Cell* 10:3081–3096.
86. Xia L, et al. (2000) Polyglycylation of tubulin is essential and affects cell motility and division in Tetrahymena thermophila. *J Cell Biol* 149:1097–1106.
87. Diz-Muñoz A, Fletcher DA, Weiner OD (2013) Use the force: Membrane tension as an organizer of cell shape and motility. *Trends Cell Biol* 23:47–53.
88. Welz T, Wellbourne-Wood J, Kerkhoff E (2014) Orchestration of cell surface proteins by Rab11. *Trends Cell Biol* 24:407–415.
89. Krtková J, Paredez AR (2017) Use of translation blocking morpholinos for gene knockdown in Giardia lamblia. *Methods Mol Biol* 1565:123–140.
90. Keister DB (1983) Axenic culture of giardia-lamblia in TYI-S-33 medium supplemented with bile. *Trans R Soc Trop Med Hyg* 77:487–488.
91. Kaplan EL, Meier P (1958) Nonparametric estimation from incomplete observations. *J Am Stat Assoc* 53:457–481.
92. Efron B, Tibshirani RJ (1994) *An Introduction to the Bootstrap* (CRC, Boca Raton, FL).
93. Sun Y, Genton MG (2011) Functional boxplots. *J Comput Graph Stat* 20:313–334.